Intercommunity resonances in multifrequency ensembles of coupled oscillators

Maxim Komarov and Arkady Pikovsky

Phys. Rev. E **92**, 012906 — Published 8 July 2015

DOI: 10.1103/PhysRevE.92.012906

Inter-community resonances in multifrequency ensembles of coupled oscillators

Maxim Komarov[1, 2, 3] and Arkady Pikovsky[1]

[1] *Department of Physics and Astronomy, University of Potsdam, Karl-Liebknecht-Str 24, D-14476, Potsdam, Germany*

[2] *Department of Cell Biology and Neuroscience, University of California Riverside, 900 University Ave. Riverside, CA 92521, USA*

[3] *Department of Control Theory, Nizhni Novgorod State University, Gagarin Av. 23, 606950, Nizhni Novgorod, Russia*

Abstract

We generalize the Kuramoto model of globally coupled oscillators to multifrequency communities. A situation when mean frequencies of two subpopulations are close to the resonance 2:1 is considered in detail. We construct uniformly rotating solutions describing synchronization inside communities and between them. Remarkably, cross-coupling across the frequencies can promote synchrony even when ensembles are separately asynchronous. We also show that the transition to synchrony due to the cross-coupling is accompanied by a huge multiplicity of distinct synchronous solutions, what is directly related to a multi-branch entrainment. On the other hand, for synchronous populations, the cross-frequency coupling can destroy phase-locking and lead to chaos of mean fields.

PACS numbers: 05.45.Xt, 05.45.-a

I. INTRODUCTION

Models in the form of coupled oscillators are ubiquitous in various scientific fields, ranging from physics and chemistry [1] to biology [2], as well as in some interdisciplinary applications [3]. In many cases the dynamics of oscillatory ensemble can be successfully studied in the phase approximation [4, 5]. When the coupling between the oscillators is relatively weak, one can neglect changes in the amplitude dynamics of natural limit cycles of the oscillators, and describe the system in terms of the phases only. This technique is known as phase reduction, and it represents, basically, one of the few rigorous mathematical approaches to study complex non-equilibrium nonlinear oscillatory dynamics.

The simplest setup here represents a globally coupled ensemble with weak interaction and relatively close natural frequencies. The phase reduction here leads to the system of globally coupled phase equations where interaction between the oscillators is described by a 2π - periodic function of phase differences [4, 6–8]. The classical and well-studied Kuramoto-Sakaguchi model appears when only the first Fourier mode in the interaction function is present, what leads to simple sinusoidal coupling. There is almost 40 years of intensive studies dedicated to explanation of bifurcations and dynamics in this model [9, 10]. A surprising recent result discovered a possibility of a low-dimensional description of the classical Kuramoto model in terms of macroscopic order parameters [11–13]. However, this reduction to low-dimensional systems does not imply simplicity of dynamical behavior. In opposite, Refs. [14] report on quite complex transitions and bifurcations in the Kuramoto-Sakaguchi models.

The cases of multi-harmonic coupling functions [8, 15] appear to be more complicated and usually responsible for new dynamical effects in comparison to the classical setup with purely sinusoidal function. In large ensembles, the multi-harmonic case leads to appearance of so-called multi-branch entrainment solutions with a huge multiplicity of possible synchronous states [8, 15, 16]. The latter also leads to non-trivial noise-induced effects [17].

One of the directions in this growing theoretical field is dedicated to *multi-frequency* oscillator communities. As it was mentioned before, the Kuramoto-type models were obtained under assumptions of weak coupling limit and closeness of natural oscillator frequencies. However, when the spreading of the frequencies is huge in comparison to the interaction strength, the phase reduction leads to another types of phase models. A natural setup here

implies existence of a certain number of oscillator subpopulations (communities), such that the frequencies inside each population are close, but differ significantly across the distinct communities [18–20]. This situation is inspired by theoretical and experimental results from neuroscience [21], indicating that distinct interacting brain areas exhibit different natural oscillatory rhythms.

In this paper we consider a particular problem when distinct oscillatory communities have natural frequencies close to a high-order resonance. First, we derive general phase equations for globally interacting ensembles and distinguish different types of resonant coupling which may appear in the system. Next, we concentrate on the simplest case of two interacting populations whose mean frequencies are close to 2:1 resonance. The aim of the paper is to demonstrate on this simplest example, what one can expect from the effects of high-order resonances. To describe the dynamics, we adapt the self-consistent approach developed in [16] for calculation of stationary order parameters for multi-harmonic coupling functions. Our analysis will show that the model exhibits reach dynamical behavior, including multi-branch entrainment (multiplicity) and chaotic collective oscillations.

II. PHASE EQUATIONS FOR RESONANTLY COUPLED POPULATIONS

In this section we will present a general scheme of coupling in resonant, multifrequency populations of oscillators. We will assume that each oscillator is described solely by its phase ϕ, which satisfies the following equation

$$\dot{\phi} = \omega + S(\phi)F \ ,$$

where ω is oscillator's natural frequency, $S(\phi)$ is its phase response curve, and F is the force acting from other oscillators. In order to simplify notations, we will consider a thermodynamic limit, where the number of units in all populations and subpopulations tends to infinity (although at the end we will also write the governing equations for a finite size case). We assume that the ensemble is divided into M distinct subpopulations (we will use index n for referring to them), around M distinct mean frequencies $\overline{\omega}_n$. Additionally, there can be a small individual deviation from the mean frequency Δ (typically described by a unimodal distribution around zero). We now introduce slow phases, by writing explicitly the fast rotating terms $\sim \overline{\omega}_n t$. In fact, we can also chose frequencies of fast rotations Ω_n to

be close, but not exactly equal, to $\overline{\omega}_n$. We will use this freedom to be able to make perfect averaging below. Our slow phases $\varphi_n(\Delta) = \phi_n - \Omega_n t$ satisfy equations

$$\dot{\varphi}_n(\Delta) = \Delta + S_n(\Omega_n t + \varphi_n) F_n \ , \tag{1}$$

where now individual mismatches Δ for the group n are distributed generally asymmetrically, with some small shift $\sim \overline{\omega}_n - \Omega_n$.

Next, we assume that coupling between the groups and inside each group is due to mean fields only. These mean fields for each subpopulation are represented by generalized order parameters

$$Z_k^{(n)} = \langle e^{ik(\Omega_n t + \varphi_n)} \rangle = \overline{Z}_k^{(n)} e^{ik\Omega_n t} \ ,$$

where averaging is over the distribution of the slow phases following from (1) and over the distribution of Δ. The introduced order parameters $\overline{Z}$ are slow functions of time as they are defined via the slow phases:

$$\overline{Z}_k^{(n)} = \langle e^{ik\varphi_n} \rangle \ . \tag{2}$$

In general, the force acting on the oscillators of the group n is from all other groups, and is a generally nonlinear function of order parameters, which one can expand in powers of them. We, however, in this paper will restrict ourselves to the linear coupling only, i.e. we will assume that F_n is a linear function of the order parameters:

$$F_n(Z_k^{(1)}, Z_k^{(2)}, \ldots) = \sum_{k,m} h_{n,k}^{(m)} Z_k^{(m)} = \sum_{k,m} h_{n,k}^{(m)} \overline{Z}_k^{(m)} e^{ik\Omega_m t} \ . \tag{3}$$

Representing the phase response function S_n as a Fourier series

$$S_n(\phi) = \sum_p s_{np} e^{ip\phi}$$

and substituting this in Eq. (1), we obtain

$$\begin{aligned} \dot{\varphi}_n(\Delta) &= \Delta + \sum_p s_{np} e^{ip\varphi} e^{ip\Omega_n t} \left[\sum_{k,m} h_{n,k}^{(m)} \overline{Z}_k^{(m)} e^{ik\Omega_m t} \right] = \\ &= \Delta + \sum_{p,k,m} s_{np} h_{n,k}^{(m)} \overline{Z}_k^{(m)} e^{ip\varphi} e^{i(p\Omega_n + k\Omega_m)t} \ . \end{aligned} \tag{4}$$

Now one has to perform averaging of Eq. (4), to reveal evolution of the slow phase. The fast terms on the r.h.s. are those containing explicit time dependence with one of the frequencies Ω_n or with a combination of them. Such a combination can be small, this is

exactly the case of a resonance that is of special interest for us. Here, we use the freedom in the choice of particular values of Ω_n, to make the resonance exact. This means that some linear combination of frequencies Ω_n vanishes exactly. Performing averaging means just keeping these terms on the r.h.s. of Eq. (4), and neglecting all other containing explicit time dependence.

Expansion (4) can be treated in many setups of particular resonant conditions, we describe here some evident cases:

- One population of oscillators. In this case only one frequency Ω exists. Here the only terms surviving the averaging are those with $p + k = 0$, this leads to the Daido model [8].

- Two subpopulations. Here the main interest is in the resonance of two frequencies Ω_1, Ω_2. The simplest case is just the second-harmonic resonance: $\Omega_2 = 2\Omega_1$. In this case only those cross-population coupling terms with $p+2k = 0$ survive. Similarly, for high-order resonances like $a\Omega_2 = b\Omega_1$ (with integer a, b) the terms with $ap + bk = 0$ contribute.

- More than two subpopulations. One can see from (4), that in the case of linear coupling, there is no direct interaction involving more than two subpopulations. So the resulting coupling is a combination of terms stemming from pairwise resonances. We mention here for completeness, that several nonlinear coupled populations of oscillators have been treated in refs. [19, 20]. In [19] three populations of oscillators have been considered, with a resonance condition $\Omega_1 + \Omega_2 = \Omega_3$, here the coupling terms contain combinations of three phases like $\phi_1 + \phi_2 - \phi_3$. In [20], a non-resonant situation has been studied, here the coupling terms are phase-independent.

We restrict ourself in this paper to the simplest case of two resonant subpopulations with $\Omega_2 = 2\Omega_1$. As described above, after averaging only terms where combinations $\sim (\Omega_{1,2} - \Omega_{1,2})$ and $\sim (\Omega_2 - 2\Omega_1)$ appear, survive, which are responsible for the interaction within one and between subpopulations, respectively:

$$\begin{aligned} \dot{\varphi}_1(\Delta) &= \Delta + \sum_k s_{1,-k} h^{(1)}_{1,k} \overline{Z}^{(1)}_k e^{-ik\varphi_1} + \sum_k s_{1,-2k} h^{(2)}_{1,k} \overline{Z}^{(2)}_k e^{-i2k\varphi_1} \ , \\ \dot{\varphi}_2(\Delta) &= \Delta + \sum_k s_{2,-k} h^{(2)}_{2,k} \overline{Z}^{(2)}_k e^{-ik\varphi_2} + \sum_k s_{2,-k} h^{(1)}_{2,2k} \overline{Z}^{(1)}_{2k} e^{-ik\varphi_2} \ . \end{aligned} \tag{5}$$

We now insert here the definition of the slow order parameters (2) and obtain

$$\begin{aligned}\dot{\varphi}_1(\Delta) &= \Delta + \langle \sum_k s_{1,-k} h^{(1)}_{1,k} e^{ik(\tilde{\varphi}_1 - \varphi_1)} \rangle + \langle \sum_k s_{1,-2k} h^{(2)}_{1,k} e^{ik(\tilde{\varphi}_2 - 2\varphi_1)} \rangle \ , \\ \dot{\varphi}_2(\Delta) &= \Delta + \langle \sum_k s_{2,-k} h^{(2)}_{2,k} e^{ik(\tilde{\varphi}_2 - \varphi_2)} \rangle + \langle \sum_k s_{2,-k} h^{(1)}_{2,2k} e^{ik(2\tilde{\varphi}_1 - \varphi_2)} \rangle \ ,\end{aligned} \tag{6}$$

where averaging is over variables with tilde. Now we can define effective coupling functions inside the subpopulations f_{11}, f_{22} and coupling functions across the subpopulation f_{12}, f_{21} as

$$\begin{aligned} f_{11}(\phi) &= \sum_k s_{1,-k} h^{(1)}_{1,k} e^{ik\phi} \ , \qquad f_{22}(\phi) = \sum_k s_{2,-k} h^{(2)}_{2,k} e^{ik\phi} \ , \\ f_{12}(\phi) &= \sum_k s_{1,-2k} h^{(2)}_{1,k} e^{ik\phi} \ , \qquad f_{21}(\phi) = \sum_k s_{2,-k} h^{(1)}_{2,2k} e^{ik\phi} \ . \end{aligned} \tag{7}$$

Now we can formulate equations for finite populations, replacing averages $\langle\rangle$ by corresponding sums. We assume that subpopulations 1 and 2 have N_1 and N_2 units, respectively. Furthermore, one can now also transform back to the original fast phases, because in the averaged formulation the absolute values of the frequencies do not play any role. Denoting the phases in the subpopulation at a smaller frequency (we will also call it the first subpopulation below) as ϕ_p, and the phases in the subpopulation at a larger double frequency (referred hereafter as the second subpopulation) as ψ_p, we get

$$\begin{aligned} \dot{\phi}_q &= \omega_q + \frac{1}{N_1} \sum_{k=1}^{N_1} f_{11}(\phi_k - \phi_q) + \frac{1}{N_2} \sum_{p=1}^{N_2} f_{12}(\psi_p - 2\phi_q) \ , \\ \dot{\psi}_q &= \nu_q + \frac{1}{N_2} \sum_{k=1}^{N_2} f_{22}(\psi_k - \psi_q) + \frac{1}{N_1} \sum_{p=1}^{N_1} f_{21}(2\phi_p - \psi_q) \ , \end{aligned} \tag{8}$$

where we also have split notations for frequencies in two subpopulations. This system is a generalization of the Daido model [8] to two resonantly coupled ensembles. Below we will consider the case where coupling functions f contain the first harmonics only; this will correspond to the Kuramoto-Sakaguchi-type coupling. In this case each coupling function is determined by two parameters, the amplitude and the phase shift. One of the phase shifts in the cross-coupling can be set to zero by shifting all the phases in one subpopulation with respect to another one. Thus, our coupling functions will be:

$$f_{11}(x) = \varepsilon_1 \sin(x - \alpha_1), \quad f_{22}(x) = \varepsilon_2 \sin(x - \alpha_2), \quad f_{12}(x) = \gamma_1 \sin(x - \beta), \quad f_{22}(x) = \gamma_2 \sin x \ .$$

Next, we fix the distributions of the frequencies. As after the averaging the system is invariant under transformation $\phi \to \phi + At$, $\psi \to \psi + 2At$ for arbitrary A, we can set the

average value of the natural frequencies in the first subpopulation ϕ to zero. Hence, the average frequency δ in the second subpopulation is the relevant parameter responsible for the frequency mismatch between the communities. We will assume that the frequencies ω and ν are distributed according to the Lorentzian distributions, with equal widths. Because we still have a freedom of changing the time scale, we will assume that this width is one:

$$g_1(\omega) = \frac{1}{\pi(\omega^2+1)} , \qquad g_2(\nu) = \frac{1}{\pi((\nu-\delta)^2+1)} . \tag{9}$$

The resulting microscopic system of oscillators to be considered below thus reads

$$\begin{aligned} \dot{\phi}_n &= \omega_n + \frac{\varepsilon_1}{N_1}\sum_{k=1}^{N_1}\sin(\phi_k - \phi_n - \alpha_1) + \frac{\gamma_1}{N_2}\sum_{k=1}^{N_2}\sin(\psi_k - 2\phi_n - \beta) , \\ \dot{\psi}_m &= \nu_m + \frac{\varepsilon_2}{N_2}\sum_{k=1}^{N_2}\sin(\psi_k - \psi_m - \alpha_2) + \frac{\gamma_2}{N_1}\sum_{k=1}^{N_1}\sin(2\phi_k - \psi_m) , \end{aligned} \tag{10}$$

with frequencies defined according to the distributions (9).

We now also write down the basic equations in the thermodynamic limit. Here three complex order parameters $\mathbf{X}_1, \mathbf{X}_2, \mathbf{Y}$ appear defined as

$$\begin{aligned} \mathbf{X}_k &= X_k e^{i\Theta_k} = \langle e^{ik\phi}\rangle = \iint d\phi d\omega \; g_1(\omega)\rho(\phi|\omega)e^{ik\phi}, \qquad k = 1, 2 , \\ \mathbf{Y} &= Y e^{i\Theta_y} = \langle e^{i\psi}\rangle = \iint d\psi d\nu \; g_2(\nu)\rho(\psi|\nu)e^{i\psi} , \end{aligned} \tag{11}$$

while equations for the phases are

$$\begin{aligned} \dot{\phi} &= \omega + \varepsilon_1 X_1 \sin(\Theta_1 - \phi - \alpha_1) + \gamma_1 Y \sin(\Theta_y - 2\phi_1 - \beta) , \\ \dot{\psi} &= \nu + \varepsilon_2 Y \sin(\Theta_y - \psi - \alpha_2) + \gamma_2 X_2 \sin(\Theta_2 - \psi) . \end{aligned} \tag{12}$$

The formulated system of equation will be subject of our analysis below, where we will concentrate on main dynamical effects caused by the resonant cross-coupling terms $\sim \gamma$. In numerical simulations we will use microscopic equations (10), while in the theoretical construction the thermodynamic limit formulation (11,12) will be used.

Before proceeding, we shortly discuss possible generalizations of the formulated equations. Generally, two subpopulations can be in a resonance $a : b$, i.e. $a\Omega_2 = b\Omega_1$. Then, instead of equations (8), one obtains

$$\begin{aligned} \dot{\phi}_q &= \omega_q + \frac{1}{N_1}\sum_{k=1}^{N_1} f_{11}(\phi_k - \phi_q) + \frac{1}{N_2}\sum_{p=1}^{N_2} f_{12}(a\psi_p - b\phi_q) , \\ \dot{\psi}_q &= \nu_q + \frac{1}{N_2}\sum_{k=1}^{N_2} f_{22}(\psi_k - \psi_q) + \frac{1}{N_1}\sum_{p=1}^{N_1} f_{21}(b\phi_p - a\psi_q) . \end{aligned} \tag{13}$$

If both $a, b > 1$, the Ott-Antonsen ansatz used below is not valid, but one can apply the self-consistent theory to find uniformly rotating synchronous states; this analysis however goes beyond the framework of this paper.

III. SELF-CONSISTENT SOLUTIONS IN THE THERMODYNAMIC LIMIT

Here we will present the self-consistent scheme allowing us to find stationary (or, more generally, uniformly rotating) synchronous solutions of the system (11,12).

A. Ott-Antonsen ansatz for the second subpopulation

The problem partially simplifies by the observation, that for the subpopulation ψ at the double frequency the Ott-Antonsen ansatz [12] can be applied. Indeed, the second of eqs. (12) can be rewritten as

$$\dot{\psi} = \nu + \mathrm{Im}(\mathbf{H}(t)e^{-i\psi}), \quad \mathbf{H} = \varepsilon_2 e^{-i\alpha_2}\mathbf{Y} + \gamma_2 \mathbf{X}_2 \; . \tag{14}$$

According to the Ott-Antonsen theory, the equation for the order parameter $\mathbf{Y}$ obeys (under some additional assumptions which we assume to be satisfied here), in the case of a Lorentzian distribution (9), an ODE

$$\dot{\mathbf{Y}} = \mathbf{Y}(i\delta - 1) - \frac{1}{2}(\mathbf{H}^*\mathbf{Y}^2 - \mathbf{H}) = \mathbf{Y}(i\delta - 1) - \frac{\varepsilon_2 \mathbf{Y}}{2}(e^{-i\alpha_2}|\mathbf{Y}|^2 - e^{i\alpha_2}) - \frac{\gamma_2}{2}(\mathbf{X}_2^*\mathbf{Y}^2 - \mathbf{X}_2) \; . \tag{15}$$

B. Uniformly rotating ansatz

We now construct a solution for the ensemble of oscillators ϕ. Here we cannot use the Ott-Antonsen ansatz, because the latter is only applicable for the driving terms possessing one harmonics of the phase, like in (14). The equations for ϕ possesses both the first and the second harmonics. In order to find stationary values of the mean fields, we will adapt the self-consistent scheme developed in Refs. [16] for the deterministic bi-harmonic Kuramoto model (for the noisy case a similar method can be used, see [17, 22]).

In this self-consistent approach one finds uniformly rotating distributions, i.e. distributions that are stationary in a rotating reference frame. Let us denote the frequency of this

frame Ω, it will be determined self-consistently as a result of the calculations. According to this, we introduce constant phases of the order parameters

$$\Theta_1 = \Omega t, \quad \theta_2 = \Theta_2 - 2\Omega t, \quad \theta_y = \Theta_y - 2\Omega t \ , \tag{16}$$

(here the phase shift of the first order parameter $\mathbf{X}_1$ is set to zero, this can be always done by the time shift). Also, we introduce a new phase variable $\varphi = \phi - \Omega t + \alpha_1$, distribution of which is expected to be stationary. This variable obeys

$$\dot{\varphi} = \omega - \Omega + \varepsilon_1 X_1 \sin(-\varphi) + \gamma_1 Y \sin(\theta_y + 2\alpha_1 - \beta - 2\varphi) \ . \tag{17}$$

C. Stationary solution in a parametric form

The structure of equation (17) for the first population is very similar to the bi-harmonic Kuramoto model considered in [16]. The difference is, that in the case of the cross-coupling, the second harmonic (the term $\sim \gamma_1$ in (17)) is proportional to the mean field of the second population Y and not to the own mean-field X_2, like in the case of the bi-harmonic Kuramoto model [16]. Nevertheless, due to the similar mathematical structure, nearly the same self-consistent method as in [16] can be adapted here. In this section we briefly outline the calculation scheme, all the details can be found in the Appendix.

First, it is convenient to introduce auxiliary parameters that directly determine the form of the phase velocity: an overall magnitude of the coupling term R, a parameter u determining relative importance of first harmonic and second harmonic terms: $\varepsilon_1 X_1 = R \sin u$, $\gamma_1 Y = R \cos u$, and a parameter $v = \theta_y + 2\alpha_1 - \beta$ determining the phase shift. Another two parameters are the rescaled rotating frequency $z = \Omega/R$ and the rescaled natural oscillator's frequency $x = \omega/R$. The form of the coupling function depends solely on u and v, in some range of these parameters (see Fig. 5 in the Appendix) and some oscillator frequencies, there are two possible stable states for the phase (due to the presence of the second Fourier mode in the coupling function). Therefore the redistribution between these states is needed, to define the distribution density of the population. This redistribution is defined by an indicator function $S(x)$ which takes values between zero and one, and can be *any* function. So, fixing $S(x)$ and parameters R, u, v, x, z one can find the distribution of the phase φ for each frequency x. Averaging the observables $e^{ik\varphi}$ over this distribution and the distribution of frequencies (needed for calculation of (11)) then reduces to calculating integrals $F_{1,2} \exp iQ_{1,2}$

as functions of $S(x)$ and parameters R, u, v, z (see eqs. (27)). Finally, the solution of the problem is represented in the parametric form: according to eqs. (28),(29), we can represent the order parameters $\mathbf{X}_{1,2}$, the frequency Ω, and the parameters of the coupling as functions of the introduced auxiliary parameters R, u, v, z, and of indicator function $S(x)$:

$$\begin{gathered} X_{1,2} = RF_{1,2}, \quad \theta_2 = Q_2 - 2\alpha_1, \quad \Omega = Rz, \quad \varepsilon_1 = \frac{\sin u}{F_1}, \\ \alpha_1 = Q_1, \quad \gamma_1 = \frac{R\cos u}{Y}, \quad \beta = \theta_y + 2Q_1 - v. \end{gathered} \tag{18}$$

D. Accounting for coupling between subpopulations

As one can see from the obtained relations (18), the parameters of the internal interaction inside the first community ε_1 and α_1 are determined unambiguously by this parametric representation. However, the constants of the cross-coupling γ_1 and β require knowledge of the order parameter $\mathbf{Y}$. Taking into account the transformation of variables (16), the uniformly rotating solution of the Ott-Antonsen equation (15) for the second population, the mean field $\mathbf{Y}$ is determined according to the following relation:

$$Ye^{i\theta_y}(i(2\Omega - \delta) + 1) + \frac{\varepsilon_2 Ye^{i\theta_y}}{2}(e^{-i\alpha_2}Y^2 - e^{i\alpha_2}) + \frac{\gamma_2 X_2}{2}(e^{-i\theta_2}Y^2e^{2i\theta_y} - e^{i\theta_2}) = 0. \tag{19}$$

This complex equation determines Y and θ_y as functions of all other parameters, substitution of these values to Eqs. (18) will give the values of cross-coupling parameters γ_1 and β.

In general case solution of (19) can not be represented in an analytic form and one should use certain numerical methods to find them (a parametric representation of solutions may be possible, but we already have four auxiliary parameters, introducing another two appears not practical). However, in two special cases equation (19) can be reduced to a simple polynomial equation with analytic solutions available. Namely, (i) for $\varepsilon_2 = 0$, the problem reduces to a complex quadratic equation, and (ii) for the special case $\Omega = \delta = 0$ and $v = 0$, equation (19) reduces to a real cubic equation. The latter case corresponds to the simplest situation when there are no phase shifts in coupling functions: $\alpha_{1,2} = \beta = 0$.

Summarizing, the self-consistent approach for calculation of stationary synchronous solutions of the problem (11,12) consists of the following steps: (i) for a given set of the parameters R, u, v, z and of the indicator function $S(x)$, one constructs the distribution function $\rho(\varphi|x)$ using microscopic dynamics (21). (ii) Next, using the function $\rho(\varphi|x)$ and equations (27,18), one determines the stationary values of order parameters $\mathbf{X}_{1,2}$, rotating

frequency Ω and corresponding coupling constants ε_1 and α_1. (iii) In the following step, one should solve equation (19) for any fixed values of ε_2, α_2, γ_2 and δ. As a result, one obtains the stationary value for the mean field $\mathbf{Y}$ and remaining constants of the cross-coupling γ_1 and β from (18).

The solution is in the parametric form: varying the set of auxiliary parameters R, u, v, z, together with ε_2, α_2 andγ_2, one gets different solutions for the mean fields $\mathbf{X}_{1,2}$, $\mathbf{Y}$, together with their dependence on the coupling constants ε_1, γ_1 and β. This can be done for any indicator function $S(x)$, which determines re-distribution of the phases of the first subpopulation between possible stable locked states, if the multi-branch entrainment is possible.

In the next sections we will apply the self-consistent scheme to characterize main types of synchronous states existing in the system of two coupled subpopulations (11,12). We will focus on the effects caused by the resonant cross coupling between the population, therefore, for the internal coupling we will consider the simplest situation when $\alpha_{1,2} = 0$. For the sake of simplicity, we restricts ourselves to the following parameters area: $\varepsilon_1 = \varepsilon_2 = \varepsilon$ and $\gamma_1 = \gamma_2 = \gamma$. It appears that the latter choice of parameters simplify the presentation of the results, nevertheless, it contains all the main effects peculiar for the high-order resonant interaction.

IV. INTERNALLY ASYNCHRONOUS POPULATIONS, APPEARANCE OF SYNCHRONY DUE TO THE RESONANT COUPLING

We start with the analysis of the case when the populations are internally asynchronous, hence, without the cross-coupling ($\gamma = 0$) the only stable state for each population is asynchrony when all mean fields vanish: $X_{1,2} = 0$, $Y = 0$. For the Lorentzian distribution of frequencies, the synchronization sets in at the critical coupling $\varepsilon = 2$. Therefore, in the following section we will concentrate on the case $\varepsilon < 2$, i.e. the internal coupling inside each population is insufficient to maintain synchrony in the system (or even is repulsive, if $\varepsilon < 0$). The frequency mismatch δ together with the cross-coupling constant γ and the phase shift β constitute a set of main control parameters in the system.

Figure 1(a) shows the area of existence of stationary synchronous solutions in the 3-d parameter space (δ, β, γ). The surface $\mathbf{M}$ depicted in the Fig. 1(a) denotes the border of existence of synchronous states: above the surface there exist stationary synchronous

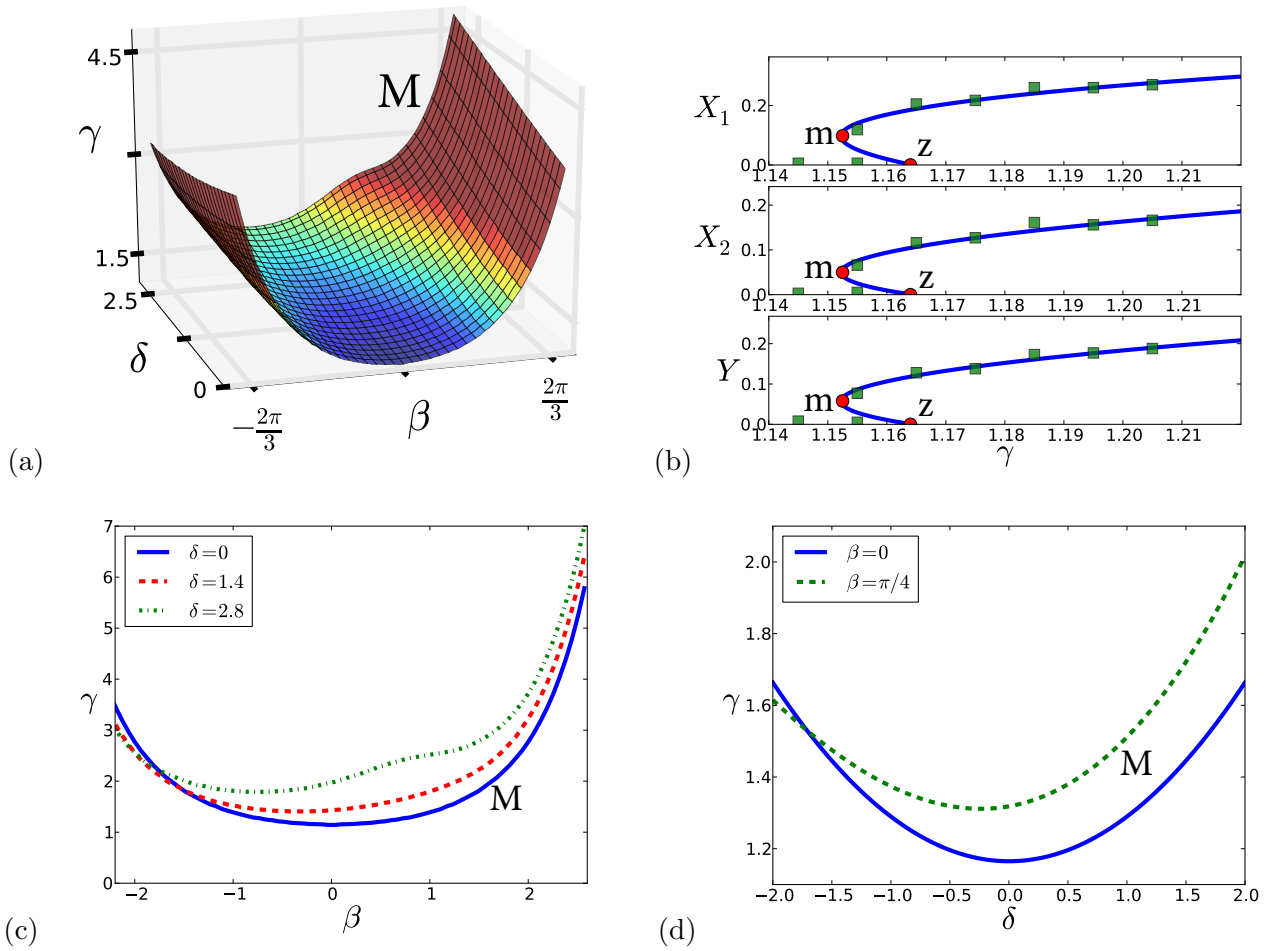

FIG. 1. (Color online) (a) The surface **M** depicts the boarder of synchronous states in the parameter space (δ, β, γ): above the surface synchrony with $X_{1,2} \neq 0$ and $Y \neq 0$ exists, below only asynchronous state is possible. The internal coupling $\varepsilon = 1$ for each population, hence, population are internally asynchronous. (b) The dependence of order parameters on the coupling constant γ is shown for $\delta = \beta = 0$ and $\varepsilon = 1$. The curves denote theoretical calculations using self-consistent scheme, markers correspond to the direct numerical calculations of the finite-size ensemble (10) for $N = 8 \times 10^5$. (c,d) Cuts of the surface **M** are shown for constant values of the frequency mismatch δ (in the panel (c)) and the phase shift β (in the panel (d)).

solutions with $X_{1,2} \neq 0$ and $Y \neq 0$, below **M** only the asynchronous state exists and is stable. Figure 1(b) explains the bifurcation diagram depicted in Fig. 1(a), here we fix the parameters $\delta = \beta = 0$ and plot the order parameters $X_{1,2}$ and Y as a function of parameter γ (the latter corresponds to the vertical line passing through the origin in the Fig. 1(a)).

As one can see from the plot, there is a minimal critical coupling γ_{cr} corresponding to the point m where two branches of synchronous solutions arise. The upper branch appears to be stable, what is confirmed by direct numerical simulation of the finite-size ensemble. The lower branch is unstable and disappears in the point z, merging with the trivial state. The family of the points m obtained at different values of β and γ constitutes the surface $\mathbf{M}$ depicted in the Fig. 1(a).

The form of the surface is invariant under transformation $\delta \to -\delta$, $\beta \to -\beta$, that is why only the part with $\delta > 0$ is shown in the Fig. 1(a). Expectedly, $\mathbf{M}$ has a global minimum at the point $\delta = \beta = 0$ what means that, substantially, the phase shift and the frequency mismatch act against synchronization. Figures 1(c,d) show several cuts of the surface $\mathbf{M}$ at constant values of $\delta = \text{const}$ (in the panel (c)) and $\beta = \text{const}$ (in the panel (d)). For the most part of the parameter range, the phase shift acts against synchronization, as one can easily see from Fig. 2(c) where the borders of stationary synchronous states are plotted on the plane (β, γ). When the frequency mismatch mismatch is absent ($\delta = 0$), the curves are symmetric with respect to the line $\beta = 0$, and the critical coupling increases with growth of the absolute value of β. However, it is not always the case for a non-zero frequency mismatch. The examples for $\delta \neq 0$ in the Fig. 2(c) clearly indicate a nontrivial fact that the global minima of the curves in the (β, γ) plane are shifted towards negative values of β. Similarly, on the (δ, γ) plane, the boarder of synchronous states has global minimum at a non-zero value of δ for finite phase shift $\beta = \pi/4$.

Remarkably, the transition to synchrony here is always accompanied by the multiplicity of different synchronous states with the multi-branch entrainment [8, 15] in the first subpopulation. The issue of multiplicity for the bi-harmonic Kuramoto model has been studied in detail in [16]. The multiple synchronous states appear as a result of strong second harmonic $\sim e^{i2\varphi}$ in the global force acting on oscillators of the first subpopulation. Apparently, in order to get a synchronization in the ensembles due to the cross-coupling, the constant γ has to be strong enough, as one can easily see from the bifurcation diagram in Fig. 1(a). The latter implies that the coupling function $h(u, v, \varphi)$ (see eq. (21)) always has a double-well form, hence, there is always a possibility to redistribute oscillators between the two stable branches in different ways (in other words, to choose an arbitrary indicator function $S(x)$ in the self-consistent scheme). As a result, for the case of internally asynchronous populations (when ε is not large enough), a family of synchronous states appears with distinct

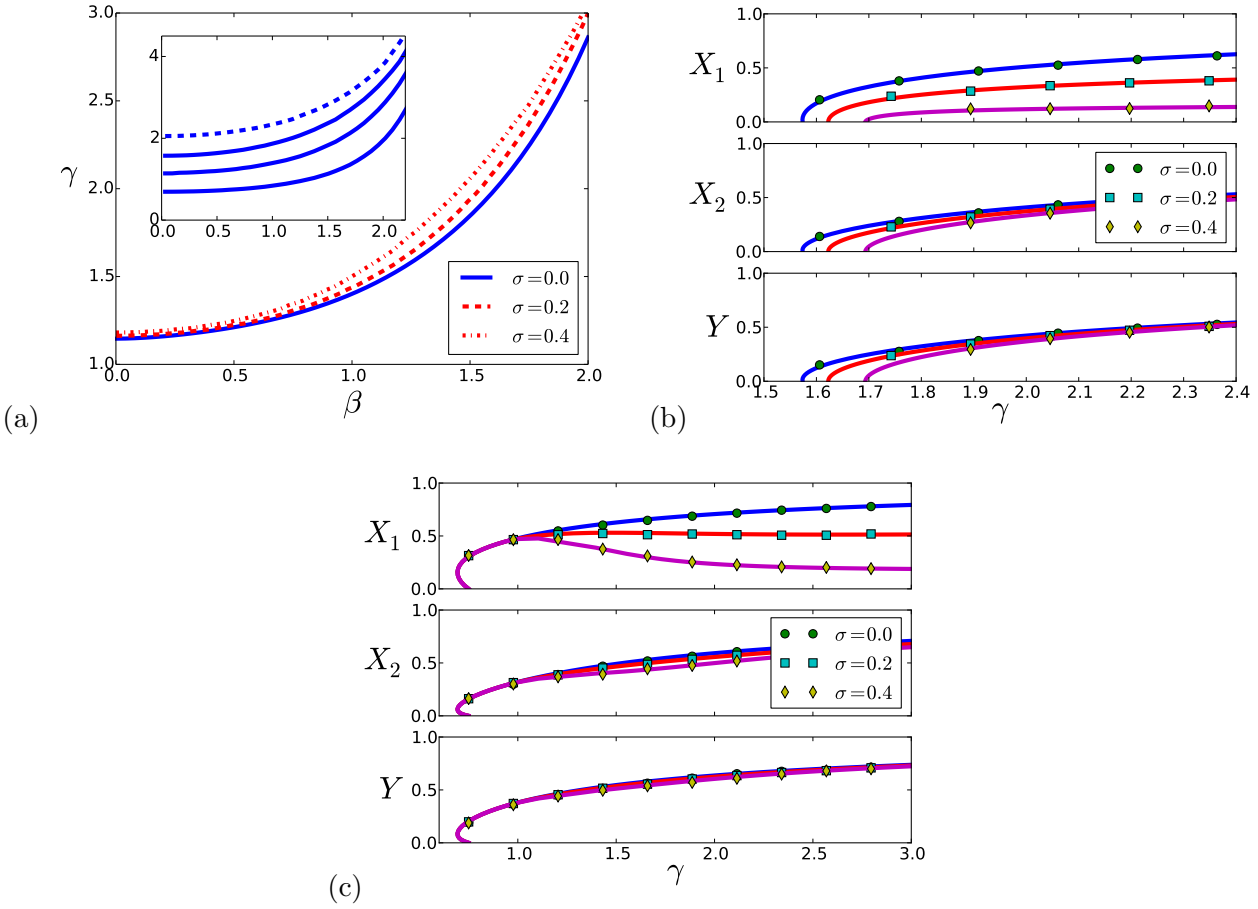

FIG. 2. (Color online) The areas of existence of stationary synchronous solutions on the parameter planes (β, γ) are shown for the case $\varepsilon = 1$ and $\delta = 0$. Different curves correspond to boarder of synchronous states with different indicator functions $S(x) = \sigma = \text{const}$ (different multi-branch entrainments). Above the curves solutions with $X_{1,2} \neq 0$, $Y \neq 0$ exist. Inset shows boundaries of synchronous states plotted for different values of constant ε. From bottom to top $\varepsilon = 1.5$, $\varepsilon = 1.0$, $\varepsilon = 0.5$, $\varepsilon = -0.1$. Note that the dashed line corresponds to the negative ε, so the internal coupling is slightly repulsive (desynchronizing) in this case. (b) Dependences of order parameters $X_{1,2}$, Y on cross-coupling γ are shown for states with different σ (see legend). Solid curves denote solutions of self-consistent equations, markers denote direct calculations of the finite-size ensemble. Other parameters are: $\varepsilon = 0.5$, $\beta = 0$, $\delta = 0$. (c) The same as (b) but for $\varepsilon = 1.5$.

multi-branch entrainments. Figure 2(a) shows the critical coupling constants γ at which synchronous states with distinct redistributions $S(x)$ appear. For the sake of simplicity we chose $S(x) = \sigma = \text{const}$. The dependences of order parameter $X_{1,2}$, Y on the cross-coupling

constant γ for different types of multi-branch entrainments (characterized by constant σ) are presented in the Fig. 1(b). The main state $\sigma = 0$ arises first (i.e. at a minimal coupling strengths γ) in comparison to other states with the multi-branch entrainments $\sigma \neq 0$. Expectedly, in all cases increase of the coupling constant γ leads to increase of the order parameters values, hence, more oscillators are entrained in both populations.

Here in this section we have concentrated on the effects caused by the cross-coupling γ and paid less attention to the role of the internal coupling ε. It is worth mentioning that, in the simplest form (pure sinusoidal coupling), the interaction inside the communities produces a relatively straightforward effect. Namely, increase of the coupling ε leads to enlargement of the area of synchrony existence in the parameter space (see inset in the Fig. 2).

V. INTERNALLY SYNCHRONOUS POPULATIONS: CHAOTIC DYNAMICS.

In this section we consider the case when $\varepsilon > 2$, hence, the populations are internally synchronous even without cross-coupling term $\sim \gamma$. Here we report on non-trivial phenomena when resonant cross-coupling yields chaotic collective oscillations.

Figure 3(a) shows the diagram of stationary synchronous states versus the phase shift in the cross-coupling function β. The solid curves correspond to solution obtained from the self-consistent approach (described above), while the markers denote direct numerical calculations of the ensemble (10) at the same parameter values. As one can easily see, the stationary states remain stable until β is less than a certain critical value (indicated by colored area in the Fig. 3(a)). However, when the phase shift becomes relatively close to π, the synchronous solutions lose stability, and immediately the system switches to a chaotic oscillation mode. The corresponding time series is presented in the Fig. 3(b). Remarkably, chaotic oscillations are characterized by a drift of the phase difference $\Delta\Theta = \Theta_2 - \Theta_y$ (see the lowest panel in the Fig. 3(b)), thus locking of the collective modes disappears. As one can easily see, the system exhibit phase slips which are indicated by jumps of the phase difference $\Delta\Theta \to \Delta\Theta \pm 2\pi$ (see transitions between the horizontal dashed lines in Fig. 3(b)). Between the slips, the phase difference exhibits oscillations with growing amplitude in the vicinity of the stationary state (horizontal dashed lines in Fig. 3(b)). Such a behavior is associated with the structure of the chaotic attractor depicted in Fig. 3(c). It appears that chaotic behavior can be described as Shilnikov chaos arising close to a homoclinic bifurcation of a

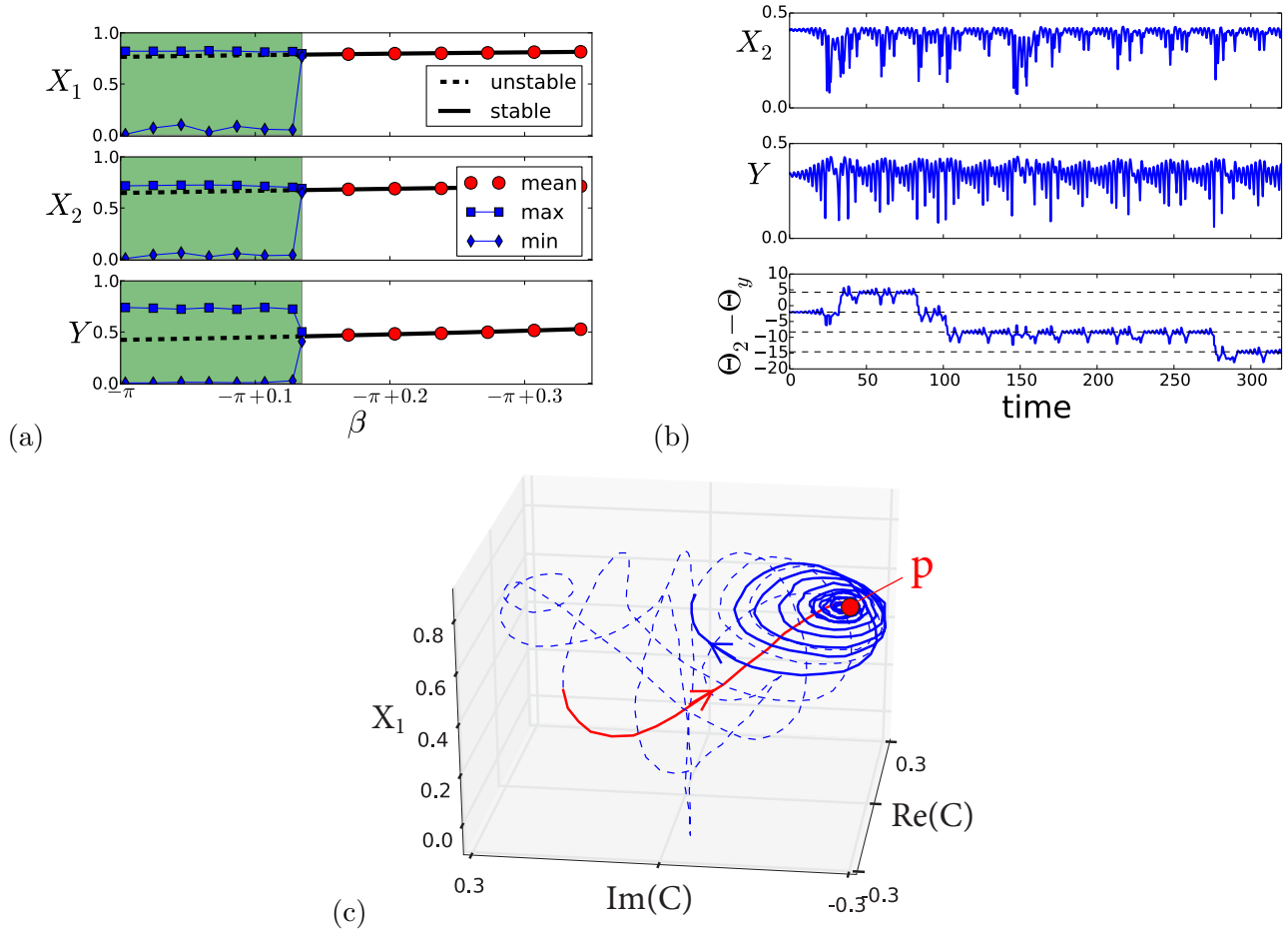

FIG. 3. (Color online) (a) Dependence of order parameters on phase shift β is presented. Solid and dashed curves denote solutions obtained from the self-consistent approach. Stable solution corresponds to solid line, unstable to dashed line (stability was checked by direct simulation of the ensemble (10)). Markers correspond to simulation of finite-size ensemble (10) for $N = 10^4$ oscillators. The colored area denotes chaotic region with large amplitude of order parameters oscillations. Parameters $\varepsilon = 4.5$, $\gamma = 2.8$. (b) Time series of the finite-size ensembles in the chaotic regime. Parameters: $\varepsilon = 4.5$, $\gamma = 2.8$, $\beta = -3.0$, $N = 10^4$. (c) Projection of the phase trajectory to the three-dimensional space where $C = YX_2^*$ (see text for details). Parameters are the same as in the panel (b).

saddle-focus equilibrium state. The steady state (point p in the Fig. 3(c)) clearly depicts a saddle-focus structure, with a two-dimensional unstable manifold (see blue solid part of the phase trajectory). Therefore, starting from the vicinity of the point p, the system exhibits growing oscillations, and then leaves a vicinity of the stationary state p. However, after

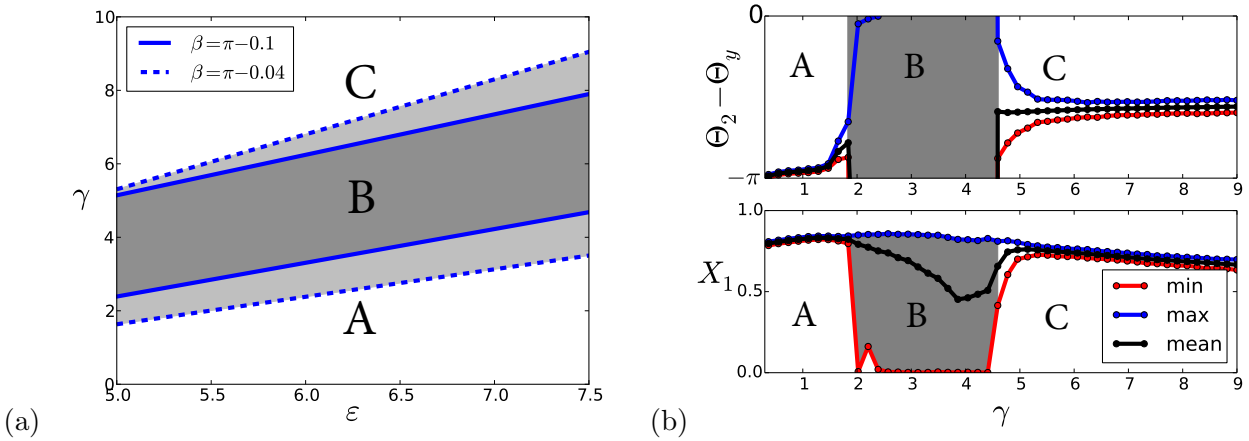

FIG. 4. (Color online) (a) The region of existence of chaotic mode on the parameter plane (ε, γ) is presented for $\beta = \pi - 0.1$, $\delta = 0$ and $N = 10^4$. (b) Dependences of the order parameter X_1 and phase difference $\Theta_2 - \Theta_y$ are presented for $\varepsilon = 5$, $\beta = \pi - 0.1$, $\delta = 0$ and $N = 10^4$. The gray area denotes asynchronous regime where the phase difference $\Theta_2 - \Theta_Y$ goes beyond the interval $[-\pi, \pi]$, so the ensembles (macroscopic order parameters) are unlocked. The latter area is characterized by irregular chaotic oscillations of macroscopic order parameters (see fig. 3(b,c)).

performing a large excursion (during which also the phase difference can change by 2π), the phase trajectory returns to a local vicinity of the point p along the stable direction (see red solid curve in the Fig. 3(c)), what gives rise to macroscopic chaotic oscillations in the system.

Fig. 4(a) is aimed to explain the structure of the parameter area where chaotic mode exists. As one can see, for each sufficiently strong internal coupling ε, there is always a certain range of cross-coupling constant γ, where oscillations are irregular. With an increase of the cross-coupling γ, the system passes from the area A (the area where regular stationary synchronous solution is stable) to area B which corresponds to chaotic motion. As has been mentioned above, area B is characterized by a drift of the phase difference and large amplitude irregular oscillations of the order parameters (see Fig. 4(b)). Further increase of constant γ leads back to a regular stationary synchronous solution (Fig. 4(b)). The size of the area B on the (ε, γ) plane is strongly related to the phase shift in coupling function: the closer is parameter β to π, the larger is area B on the (ε, γ) plane. One can conclude that for chaos and desynchronization to occur, presence of the phase shift β in the coupling function is essential. It is worth mentioning, that the chaotic mode observed in direct simulations

appears to be weakly dependent on the system size N, if the latter is large. Calculations with $N = 10^3$ and $N = 5 \times 10^2$ reveal almost the same boundaries of existence (Fig. 4) and similar dynamical properties. However, for smaller ensembles ($N \approx 10^2$), strong finite-size fluctuations interfere with the chaotic dynamics and may cause large differences in the structure of parameter space and dynamics.

VI. CONCLUSIONS

The phase reduction is one of the few mathematical techniques which allows one to perform analytical studies of complex nonlinear oscillatory systems. Perhaps, the most popular and well-studied phase model is the classical Kuramoto system which describes ensemble of globally coupled oscillators with sinusoidal type of interaction function. The derivation of various Kuramoto-type models is based on the assumption of closeness of natural oscillatory frequencies. However, in many realistic situations oscillators may have definitely different frequencies; an example of this are neural populations that can produce brain waves wide across the spectrum. For multifrequency populations one has to extend basic models of phase dynamics; in previously considered cases such an extension also led to new dynamical regimes [19, 20].

In the present paper we developed an extension of the phase synchronization theory for multifrequency *resonant* oscillator communities. After analyzing general possible resonant terms for linear mean-field coupling, we focused on the simplest high-order resonant case, when two communities of oscillators are globally coupled and have natural population frequencies close to the rational relation 2:1. First, given the assumption on mean population frequencies, we derived the simplest form of phase equations for the high-order resonant interaction between two globally coupled communities of oscillators. Basically, the structure of the model consists of two main parts: the first part represents the standard sinusoidal term describing Kuramoto-type interaction inside each community; the second component represents resonant cross-coupling between the populations. Next, we combine two approaches described in Refs. [16] and in Refs. [12] to derive a self-consistent scheme allowing us calculation of stationary synchronous solutions of the system in the thermodynamic limit.

In this paper we focused on studying how cross-coupling promotes synchronization, and looked for novel dynamical effects due to the high-order resonance. Hence, we have con-

sidered two qualitatively different cases, in the first case the populations were internally asynchronous, so, the internal coupling strength was relatively weak or repulsive. Here we constructed the bifurcation diagram showing how synchronous regimes appear in dependence on main parameters of the model. We demonstrated, that strong enough resonant cross-coupling results in stationary synchronous solutions appearing in both subpopulations. Thus, the synchrony can be only mutual. The nontrivial fact here is that the transition to synchrony due to the cross-coupling is always accompanied by multiplicity of distinct synchronous states, similar to the case of the bi-harmonic Kuramoto model [16]. In the second setup, we considered an opposite situation, when the internal coupling is strong, such that almost all oscillators are locked to the mean fields in the absence of the cross-coupling. Here we report on a quite non-trivial effect, that the asymmetric cross-coupling can destroy the stationary synchronous state introducing chaos into the system. The mean fields of two subpopulations not only demonstrate chaotically varying amplitudes, but the subpopulations also desynchronize from each other in the sense, that the phase shift between the mean fields is no more a constant, but performs a biased random walk.

VII. ACKNOWLEDGEMENT

M. K. thanks Alexander von Humboldt Foundation, NIH (R01 DC012943) and ONR (N000141310672) for support. The research in sections IV and V was supported by the Russian Science Foundation (Project 14-12-00811).

APPENDIX

To proceed with self-consistent solution of Eq. (17), it is convenient to introduce four auxiliary parameters $\{R,\ u,\ v,\ z\} = \mathbf{P}$ in the following way:

$$\varepsilon_1 X_1 = R\sin u,\ \gamma_1 Y = R\cos u,\ \Omega = zR,\ v = \theta_y + 2\alpha_1 - \beta\ . \tag{20}$$

Now (17) takes the following form:

$$\dot{\varphi} = R\left(x - z - \sin u\sin\varphi - \cos u\sin(2\varphi - v)\right) = R\left(x - z - h(u, v, \varphi)\right)\ . \tag{21}$$

We denoted $x = \omega/R$ and $h(u, v, \varphi) = \sin u\sin\varphi + \cos u\sin(2\varphi - v)$. The new variables and parameters have the following meaning (which is very similar for the bi-harmonic case [16]):

- θ_2 and θ_y are stationary phases of the first (mean field $\mathbf{X}_2$) and the second populations correspondingly.

- $R = \sqrt{\varepsilon_1^2 X_1^2 + \gamma_1^2 Y^2}$ is an overall magnitude of the interaction function for the first population. Roughly speaking, relatively large values of R indicate coherent dynamics with relatively high amplitudes X_1 and/or Y. $R = 0$ means vanishing order parameters $X_1 = Y = 0$, what corresponds to complete asynchrony.

- u is a parameter reflecting relative strengths of coupling terms in the first and the second harmonics: ($\sin u = \frac{\varepsilon X_1}{R}$ and $\cos u = \frac{\gamma_1 Y}{R}$, respectively).

- $z = \Omega/R$ is the rescaled rotating frequency of the order parameters.

- $x = \omega/R$ is the rescaled individual frequencies of oscillators.

- $v = \theta_y + 2\alpha_1 - \beta$ is an effective phase shift of the second harmonics coupling term with respect to the coupling at the first harmonics.

- $h(u, v, \varphi) = \sin u \sin\varphi + \cos u \sin(2\varphi - v)$ is the rescaled coupling function.

At some constant values of parameters $\mathbf{P}$ in (21), at each value of x one can find stationary distribution function $\rho(\varphi|x, \mathbf{P})$, and then calculate the corresponding complex order parameters:

$$\begin{aligned} X_1 &= e^{-i\alpha_1} R \iint \rho(\varphi|x,\mathbf{P}) e^{i\varphi} g(Rx) dx d\varphi = e^{-i\alpha_1} R F_1(\mathbf{P}) e^{iQ_1(\mathbf{P})} \\ X_2 e^{i\theta_2} &= e^{-i2\alpha_1} R \iint \rho(\varphi|x,\mathbf{P}) e^{i2\varphi} g(Rx) dx d\varphi = e^{-i2\alpha_1} R F_2(\mathbf{P}) e^{iQ_2(\mathbf{P})} \\ F_m(\mathbf{P}) e^{iQ_m(\mathbf{P})} &\equiv \iint dx d\varphi \rho(\varphi|x,\mathbf{P}) e^{im\varphi} g(Rx) \ , \qquad m = 1, 2 \ . \end{aligned} \tag{22}$$

Our next goal is to calculate the integrals $F_m(\mathbf{P})$, for this we need to find, using the dynamical equation (21), the stationary distribution function $\rho(\varphi|x, \mathbf{P})$. Let H_{min} and H_{max} denote the global minimum and the global maximum of function $h(u, v, \varphi)$, correspondingly (Fig.5(b)). All the oscillators can be separated into locked ones (for $H_{max} \geq x - z \geq H_{min}$) or rotating, unlocked ones ($x - z > H_{max}$ or $x - z < H_{min}$). The distribution function of rotating oscillators (index r) is inversely proportional to their phase velocity:

$$\rho_r(\varphi|x, \mathbf{P}) = \frac{C(x)}{|x - z - h(\varphi, u, v)|} \ , \tag{23}$$

where $C(x)$ is the normalization constant:

$$C(x) = \frac{1}{\int_0^{2\pi} \frac{d\varphi}{|x-z-y|}}.$$

The stationary phases of locked oscillators (index l) can be found from the following relation:

$$x - z = h(u, v, \varphi) \ . \tag{24}$$

When finding φ as a function of x for non-rotating (locked, index l) phases, we have to satisfy an additional stability condition $\frac{\partial h(u,v,\varphi)}{\partial \varphi} > 0$, that follows from the dynamical equation (21). In the (u, v) plane there are two regions V_1 and V_2 (Fig. 5(a)) with qualitatively different properties of the system (21) and different types of distribution function $\rho_l(\varphi|x, \mathbf{P})$, correspondingly:

a. $\{u, v\} \in V_1$ In this case function $h(u, v, \varphi)$ has a double-well form like shown in Fig.5(b). According to (21), oscillators can be located on two possible stable branches highlighted by solid curves in Fig.5(b): the first branch is $\varphi = \Psi_1(x, \mathbf{P})$ in the range $\varphi \in [\varphi_1, \varphi_2]$ and another branch is $\varphi = \Psi_2(x, \mathbf{P})$ for $\varphi \in [\varphi_3, \varphi_4]$. Here and below we assume $\Psi_1(x, \mathbf{P})$ to be the biggest stable branch. In the range $(x-z) \in (x_1^b, x_2^b)$ (Fig. 5(b)) there is an area of bistability on the microscopic level: the oscillators with the same natural frequency x can be locked at two different phases $\Psi_1(x, \mathbf{P})$ and $\Psi_2(x, \mathbf{P})$. Therefore, the distribution function has the following form:

$$\rho_l(\varphi|x, \mathbf{P}) = \begin{cases} (1 - S(x))\delta(\psi - \Psi_1(x, \mathbf{P})) + S(x)\delta(\varphi - \Psi_2(x, \mathbf{P})) \\ \text{for } (x - z) \in [x_1^b, x_2^b] \ , \\ \delta(\varphi - \Psi_1(x, \mathbf{P})) \quad \text{for } (x - z) \in [x_1, x_2] \setminus [x_1^b, x_2^b] \ , \\ \delta(\varphi - \Psi_2(x, \mathbf{P})) \quad \text{for } (x - z) \in [x_3, x_4] \setminus [x_1^b, x_2^b] \ . \end{cases} \tag{25}$$

Here $0 \leq S(x) \leq 1$ is an indicator function describing the redistribution over the stable brunches; this function is arbitrary.

b. $\{u, v\} \in V_2$ In the second case, function $h(u, v, \psi)$ has only two extrema (Fig. 5(c)) and there is only one stable branch $\varphi = \Psi_1(x, \mathbf{P})$. The distribution function is:

$$\rho_l(\varphi|x, \mathbf{P}) = \delta(\varphi - \Psi_1(x, \mathbf{P})) \text{ for } x \in (z + x_1, z + x_2) \ . \tag{26}$$

Taking into account the obtained expressions for the distribution function (23,25,26), the

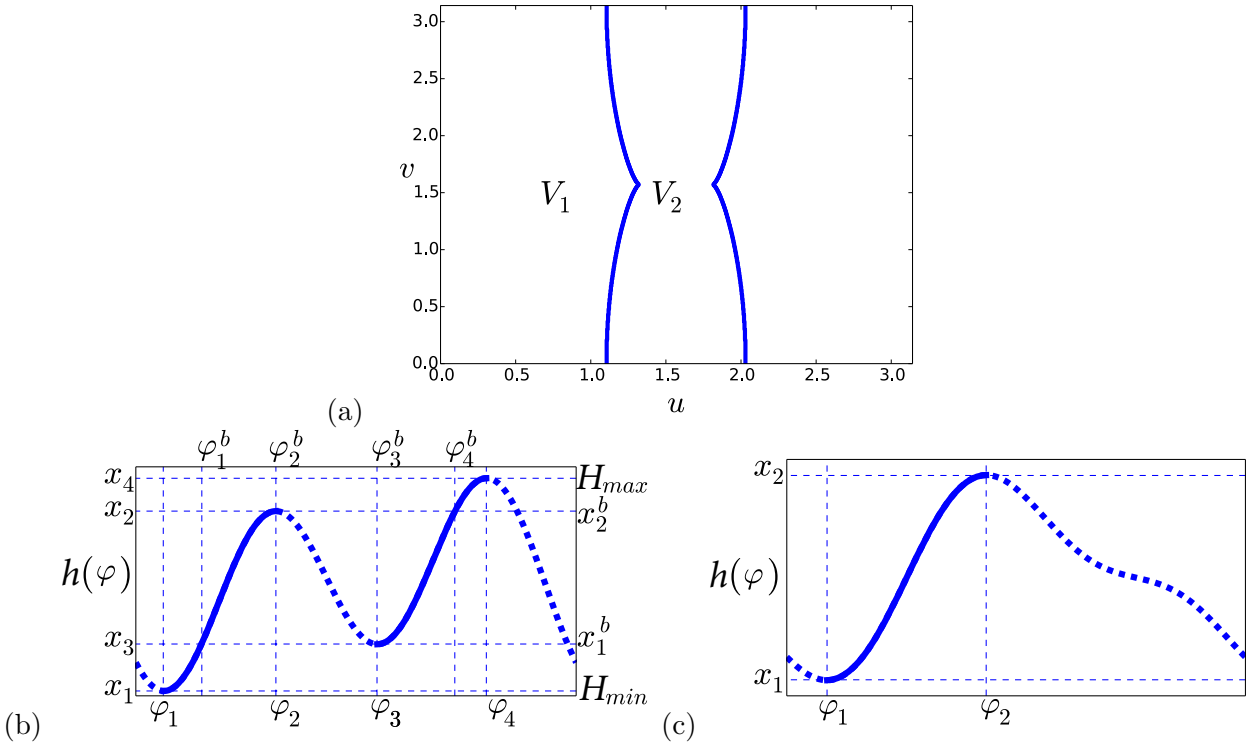

FIG. 5. (a) Regions V_1 and V_2 in the plane of parameters (u, v): Domain V_1 corresponds to a double-well form of function $h(u, v, \varphi)$ (Fig. 5(b,d)), while in V_2 $h(u, v, \varphi)$ has a single-well form like sown in Fig. 5(c). (b) Example of function $h(u, v, \varphi)$ with 4 extrema is presented. There are two stable branches (solid curves) for stationary phases of locked oscillators. The left branch $\varphi = \Psi_1(x, \mathbf{P})$ is larger than the right one $\varphi = \Psi_2(x, \mathbf{P})$. $(\varphi_{1,2}, x_{1,2})$ denote coordinates of the extrema corresponding to the branch Ψ_1, while $(\varphi_{3,4}, x_{3,4})$ denotes extrema at Ψ_2. In the domain $h(\varphi) \in [x_1^b, x_2^b]$ there is a bistability on the microscopic level: in this domain the oscillators can be locked either on the branch Ψ_1 in the range $\varphi \in [\varphi_1^b, \varphi_2^b]$ or on the branch Ψ_2 in the range $\varphi \in [\varphi_3^b, \varphi_4^b]$. (c) Example of function $h(u, v, \varphi)$ with only two extrema and one stable branch $\varphi = \Psi_1(x, \mathbf{P})$ (solid curve).

integrals in (22) can be rewritten as a sum of five terms:

$$F_m(\mathbf{P})e^{iQ_m(\mathbf{P})} = \int_{\varphi_1}^{\varphi_2} d\varphi e^{im\varphi} g\left(R(z+h)\right) \frac{\partial h}{\partial \varphi} - \int_{\varphi_1^b}^{\varphi_2^b} d\varphi e^{im\varphi} S(z+h) g\left(R(z+h)\right) \frac{\partial h}{\partial \varphi} + \int_{\varphi_3}^{\varphi_4} d\varphi e^{im\varphi} g\left(R(z+h)\right) \frac{\partial h}{\partial \varphi} - \int_{\varphi_3^b}^{\varphi_4^b} d\varphi e^{im\varphi} \left(1 - S(z+h)\right) g\left(R(z+h)\right) \frac{\partial h}{\partial \varphi} + \int_{\mathcal{X}} \int_0^{2\pi} dx d\varphi \frac{g(Rx) C(x) e^{im\varphi}}{|x - z - h|} . \tag{27}$$

Here the first and the second terms stand for integration over the first branch Ψ_1 in the range $[\varphi_1, \varphi_2]$. The second term accounts for certain redistribution $S(x)$ of oscillators between the branches in the range $[\varphi_1^b, \varphi_2^b]$ (Fig. 5(b)). Similarly, the third and the fourth terms correspond to integration over the possible stable branch Ψ_2 in the range $[\varphi_3, \varphi_4]$. In the same way, the fourth term accounts for redistribution of oscillators between branches in the range $[\varphi_3^b, \varphi_4^b]$ (Fig. 5(b)). In the last term the interval $\mathcal{X} = (-\infty, z + H_{min}) \bigcup (z + H_{max}, \infty)$ is the domain of frequencies where the oscillators are not locked.

Thus, the order parameters $\mathbf{X}_{1,2}$ and the frequency Ω as functions of introduced auxiliary parameters R, u, v, z:

$$X_{1,2}(\mathbf{P}) = RF_{1,2}(\mathbf{P}), \quad \theta_2 = Q_2(\mathbf{P}) - 2\alpha_1, \quad \Omega(\mathbf{P}) = Rz \; . \tag{28}$$

Also, from the relations (20,22) one can conclude that the following holds:

$$\varepsilon_1 = \frac{\sin u}{F_1(\mathbf{P})}, \quad \alpha_1 = Q_1(\mathbf{P}), \quad \gamma_1 = \frac{R\cos u}{Y}, \quad \beta = \theta_y + 2Q_1(\mathbf{P}) - v. \tag{29}$$

---

[1] K. Wiesenfeld and J. W. Swift, Phys. Rev. E **51**, 1020 (1995); K. Wiesenfeld, P. Colet, and S. H. Strogatz, Phys. Rev. Lett. **76**, 404 (1996); K. Wiesenfeld, P. Colet, and S. Strogatz, Physical Review E **57**, 1563 (1998); I. Kiss, Y. Zhai, and J. Hudson, Science **296**, 1676 (2002); J. Grollier, V. Cros, and A. Fert, Phys. Rev. B **73**, 060409(R) (2006); B. Georges, J. Grollier, V. Cros, and A. Fert, Appl. Phys. Lett. **92**, 232504 (2008).

[2] D. Golomb, D. Hansel, and G. Mato, in *Neuro-informatics and Neural Modeling*, Handbook of Biological Physics, Vol. 4, edited by F. Moss and S. Gielen (Elsevier, Amsterdam, 2001) pp. 887–968; M. Breakspear, S. Heitmann, and A. Daffertshofer, Frontiers in human neuroscience **4**, 190 (2010); D. Gonze, S. Bernard, C. Waltermann, A. Kramer, and H. Herzel, Biophysical Journal **89**, 120 (2005); G. Bordyugov, P. Westermark, A. Korencic, and H. Herzel, in *Circadian Clocks*, edited by A. Kramer and M. Merrow (Springer, 2013).

[3] B. Eckhardt, E. Ott, S. H. Strogatz, D. M. Abrams, and A. McRobie, Phys. Rev. E **75**, 021110 (2007); Z. Néda, E. Ravasz, T. Vicsek, Y. Brechet, and A. L. Barabási, *ibid.* **61**, 6987 (2000).

[4] Y. Kuramoto, *Chemical Oscillations, Waves and Turbulence* (Springer, Berlin, 1984).

[5] A. Pikovsky, M. Rosenblum, and J. Kurths, *Synchronization. A Universal Concept in Nonlinear Sciences.* (Cambridge University Press, Cambridge, 2001).

[6] Y. Kuramoto, in *International Symposium on Mathematical Problems in Theoretical Physics*, edited by H. Araki (Springer Lecture Notes Phys., v. 39, New York, 1975) p. 420.

[7] E. M. Izhikevich, *Dynamical Systems in Neuroscience* (MIT Press, Cambridge, Mass., 2007); SIAM Journal on Applied Mathematics **60**, 1789 (2000).

[8] H. Daido, Physica D **69**, 394 (1993); Prog. Theor. Phys. **89**, 929 (1993); Physica D **91**, 24 (1996); J. Phys. A: Math. Gen. **28**, L151 (1995).

[9] J. A. Acebrón, L. L. Bonilla, C. J. P. Vicente, F. Ritort, and R. Spigler, Rev. Mod. Phys. **77**, 137 (2005).

[10] A. Pikovsky and M. Rosenblum, arXiv:1504.06747 [nlin.AO] (2015).

[11] S. Watanabe and S. H. Strogatz, Physica D **74**, 197 (1994).

[12] E. Ott and T. M. Antonsen, CHAOS **18**, 037113 (2008); CHAOS **19**, 023117 (2009).

[13] S. A. Marvel, R. E. Mirollo, and S. H. Strogatz, Chaos **19**, 043104. (2009); A. Pikovsky and M. Rosenblum, Phys. Rev. Lett. **101**, 264103 (2008); Physica D **240**, 872 (2011).

[14] O. E. Omel'chenko and M. Wolfrum, Phys. Rev. Lett. **109**, 164101 (2012); Physica D **263**, 74 (2013).

[15] H. Daido, Phys. Rev. Lett. **77**, 1406 (1996); J. D. Crawford, **74**, 4341 (1995); J. D. Crawford and K. T. R. Davies, Physica D **125**, 1 (1999); H. Chiba and I. Nishikawa, Chaos **21**, 043103 (2011); D. Hansel, G. Mato, and C. Meunier, Phys. Rev. E **48**, 3470 (1993); P. Ashwin, G. Orosz, J. Wordsworth, and S. Townley, SIAM Journal on Applied Dynamical Systems **6**, 728 (2007).

[16] M. Komarov and A. Pikovsky, Phys. Rev. Lett. **111**, 204101 (2013); Physica D **289**, 18 (2014).

[17] V. Vlasov, M. Komarov, and A. Pikovsky, J. Phys. A: Mathematical and Theoretical **48**, 105101 (2015).

[18] S. Lück and A. Pikovsky, Physics Letters A **375**, 2714 (2011).

[19] M. Komarov and A. Pikovsky, Phys. Rev. Lett. **110**, 134101 (2013).

[20] M. Komarov and A. Pikovsky, Phys. Rev. E **84**, 016210 (2011).

[21] G. Buzsáki, *Rhythms of the brain* (Oxford UP, Oxford, 2006); N. Rosjat, S. Popovych, and S. Daun-Gruhn, Theoretical Biology and Medical Modelling **11** (2014).

[22] M. Komarov, S. Gupta, and A. Pikovsky, EPL **106**, 40003 (2014).